

# Accuracy Assessment of MODIS Land Aerosol Optical Thickness Algorithms using AERONET Measurements over North America

5 Hiren Jethva<sup>1,2</sup>, Omar Torres<sup>2</sup>, Yasuko Yoshida<sup>1,3</sup>

<sup>1</sup>Universities Space Research Association, 7178 Columbia Gateway Drive, Columbia, MD 21046, USA

<sup>2</sup>NASA Goddard Space Flight Center, Earth Science Division, Code 614, Greenbelt, MD 20771, USA

<sup>3</sup>Science Systems and Applications, Inc., 10210 Greenbelt Rd, Lanham, MD 20706 USA

10

## Abstract

The planned simultaneous availability of visible and near-IR observations from the geostationary platforms of Tropospheric Emissions: Monitoring of Pollution (TEMPO) and Geostationary Operational Environmental Satellites (GOES) 16/17 Advanced Base Imager (ABI) will present the opportunity of deriving an accurate aerosol product taking advantage of both ABI's high spatial resolution in the visible and TEMPO's sensitivity to aerosol absorption in the near-UV. Because the wavelengths of ABI's are similar to those of the Moderate Resolution Imaging Spectroradiometer (MODIS), existing aerosol algorithms of MODIS can be applied to ABI observations. In this work, we evaluate three distinct aerosol algorithms of MODIS deriving aerosol optical thickness (AOT) over land surfaces using visible and near-IR observations. The Dark Target (DT), Deep Blue (DB), and Multiangle Implementation of Atmospheric Correction (MAIAC) algorithms are all applied to the radiance measurements of MODIS onboard Aqua satellite. We have evaluated each algorithm by comparing the satellite-retrieved AOT to space-time collocated ground-based sunphotometer measurements of the same parameter at 171 sites of the Aerosol Robotic Network (AERONET) over North America (NA). A spatiotemporal scheme co-locating the satellite retrievals with the ground-based measurements was applied consistently to all three retrieval datasets. We find that the statistical performance of all three algorithms is comparable over darker surfaces over eastern NA with the MAIAC algorithm provides relatively better comparison over western NA sites characterized by inhomogeneous elevation and bright surfaces. The higher spatial resolution of MAIAC product (1 km) allows a substantially larger

30

number of matchups than DB 10-km and DT 10-km (DT 3-km) products by 115% and 120% (86%) respectively over Eastern NA, and by 150% and 220% (197%) over Western NA. The characterization of error in AOT for the three aerosol products as a function of both MAIAC-retrieved and an independent MOD09 atmospheric correction derived bi-directional surface reflectance shows a systematic positive bias in DT retrievals over brighter surfaces, whereas DB and MAIAC retrievals show no such bias throughout the wide range of surface brightness with MAIAC offering lowest spread in errors. The results reported here represent an objective, unbiased evaluation of existing over-land aerosol retrieval algorithms of MODIS. The detailed statistical evaluation of the performance of each of these three algorithms may be used as guidance in the development of inversion schemes to derive aerosol properties from ABI or other MODIS-like sensors.

**Keywords:** aerosol optical thickness, MODIS, Dark Target, Deep Blue, MAIAC, AERONET, North America

# 1. Introduction

The Tropospheric Emissions: Monitoring of Pollution (TEMPO) mission is NASA's first Earth Venture Instrument (Zoogman *et al.*, 2017). It will be hosted on a still undetermined geostationary satellite with an estimated earliest launch in 2020. TEMPO's hyperspectral observations in the 290-490 nm and 540-740 nm wavelength ranges (0.6 nm spectral resolution) will measure trace gas concentrations (O<sub>3</sub>, NO<sub>2</sub>, SO<sub>2</sub>, CH<sub>2</sub>O, and others) and suspended particle matter (PM). Spatial coverage includes most of Canada, the Contiguous United States (CONUS), Northern Mexico, and part of the Caribbean at an approximate spatial resolution of 2.1x4.7 km<sup>2</sup>. TEMPO partially fulfills the objectives of the Geostationary Coastal and Air Pollution Events (GEO-CAPE) mission recommended by National Research Council's Earth Science Decadal Survey to measure tropospheric gases, aerosols, and coastal phytoplankton to monitor air and water quality (Fishman *et al.*, 2012).

Accurate characterization of the tropospheric aerosol load is required as input to a particulate matter (PM) computational scheme along with meteorological information such as temperature and pressure profiles, relative humidity, and planetary boundary layer (PBL) height. The simultaneous availability on GEO platforms of TEMPO and GOES 16/17 Advanced Baseline Imager (ABI) observations in the visible and near-IR present the opportunity of deriving an accurate aerosol product taking advantage of both ABI's high spatial resolution in the visible and near-IR, and TEMPO's sensitivity to aerosol absorption in the near-UV. The combination of 500 m to 2 km spatial resolutions and multispectral observations in the visible to shortwave-IR make the ABI an optimum sensor for the derivation of an aerosol optical thickness (AOT) product over land at the GEO-CAPE required accuracy (Fishman *et al.*, 2012) to be used in conjunction with TEMPO observations for air quality and climate applications.

Satellite-based aerosol remote sensing has been an essential tool to monitor the spatial and temporal distributions of aerosols globally. Significant advancements in aerosol retrieval capabilities over both land and ocean have taken place over the last 20 years. The deployment of the Moderate Resolution Imaging Spectroradiometer (MODIS) and the Multi-angle Imaging Spectroradiometer (MISR) on board the Earth Observing System (EOS) Terra (1999) satellite and a second identical MODIS sensor on the Aqua (2002) platform marked the beginning of a

new era in space-based aerosol remote sensing. AOT is routinely derived from MODIS observations by three distinct and independent algorithms: Dark Target algorithm (*Remer et al.*, 2005; *Levy et al.*, 2007; 2013), Deep Blue algorithm (*Hsu et al.*, 2004, 2013), and the Multi-Angle Implementation of Atmospheric Correction (MAIAC) algorithm (*Lyapustin et al.*, 2011, 5 2018).

In this paper, we evaluate the accuracy of the available multi-year long records of AOT products derived by the three MODIS algorithms by a direct comparison to ground-based observations from the Aerosol Robotic Network (AERONET) at multiple sites in North America-an area or regard for both ABI and TEMPO field-of-views. A brief description of MODIS aerosol 10 algorithms, their products, and satellite-ground collocation procedure are given in section 2. The results of the satellite-ground comparison of individual sites, composites of all sites, and error characterization are presented in section 3, followed by concluding remarks given in section 4.

## 2. Datasets and Collocation Strategy

### 2.1 MODIS Dark Target Aerosol Product

15 The dark target (DT) algorithm of MODIS consists of two separate algorithms, a land component for the retrieval of aerosol properties over vegetated surfaces, and an over-ocean retrieval algorithm. The over-land DT algorithm exploits the top-of-atmosphere (TOA) reflectance measurements in three MODIS bands, i.e., 470 nm, 670 nm, and 2130 nm to simultaneously derive AOT at all three channels with an underlying assumption that the impact of fine mode 20 aerosols on 2130 nm signal is ignorable, and that the 2130 nm channel contains information about coarse mode aerosol as well as the surface reflectance. The surface characterization is achieved through linear regression of surface reflectance in the 2130 nm and visible channels (470 nm, 670 nm) (*Kaufman et al.* 1997; *Remer et al.*, 2005) accounting for the viewing geometry and “greenness” of land cover (*Levy et al.*, 2007). DT attempts to perform retrieval on 25 each 10 km grid box using a limited number of TOA reflectance observations after discarding 50% brightest, 20% darkest, and cloudy pixels out of a total 400 pixels at 500 meters resolution at nadir. The DT over-land algorithm screens cloudy pixels following a series of tests that rely on using absolute magnitude and spatial variability at 470 nm (500 m resolution) and 1380 nm (1 km resolution), the details of which are given in *Martins et al.*, (2002) and *Levy et al.*, (2013).

DT is essentially a look-up table search algorithm which combines the pre-calculated spectral reflectance of the location-time dependent aerosol models comprised of dominant fine and coarse modes with a proper weighting to represent the ambient aerosol properties over the target. The weighted-average spectral LUT reflectance values are compared against the TOA spectral measurements of MODIS to find the best match in AOT yielding least square difference between simulated and observed reflectances. Each valid retrieval is assigned with a quality assurance confidence flag (QAC) with best retrievals tagged as QAC=3. Over land, the expected error for AOT (0.55  $\mu\text{m}$ ) with QAC=3 is estimated to be  $\pm(0.05+15\%)$ , whereas that over ocean is  $\pm(0.03+5\%)$  for retrievals with  $\text{QAC} \geq 1$ . A detailed description of the DT Collection 6 algorithm is given in *Levy et al.* (2013) and also available online at URL <https://darktarget.gsfc.nasa.gov/>.

In addition to the 10-km AOT product, the MODIS DT algorithm also offers a higher resolution aerosol product at 3-km spatial scale. While both aerosol products closely resemble each other, the 3-km product differs from the original 10-km product in the manner in which the MODIS pixels are ingested, organized, and selected by the aerosol algorithm (*Remer et al.*, 2013). The expected error associated with the 3-km aerosol retrievals over land globally is found to be 0.01 to 0.02 higher than that of the 10-km product (*Remer et al.*, 2013).

## 2.2 MODIS Deep-blue Aerosol Product

The MODIS deep-blue (DB) aerosol algorithm utilizes the radiance measurements at the blue wavelength (412 nm), where the surface reflectance over land is relatively lower than that at longer visible wavelengths, to retrieve the column AOT over bright surfaces (*Hsu et al.*, 2004) as well as vegetated areas (*Hsu et al.*, 2013). The surface characterization scheme of DB adopts a hybrid approach that applies the dynamical surface reflectance method for urban built-up and the precalculated surface reflectance database in conjunction with the normalized vegetation index in arid and semi-arid areas (*Hsu et al.*, 2013). The dynamical surface reflectance method allows larger spatial coverage of DB aerosol product by expanding the retrieval capability from the bright surfaces to all snow-free land surfaces, including vegetated areas. The surface reflectance dataset used in the DB algorithm is created from the full time-series and revised during each reprocessing. The surface dataset is essentially based on minimum reflectivity approach and binned by scattering angle, season, and NDVI with no time dimension except for the seasonal split. Over vegetated surfaces, DB follows the spectral ratio approach similar to that of DT. The

hybrid method scales surface reflectance by regional BRDF shape, based on atmospheric correction near AERONET sites. The enhanced second generation of DB algorithm identifies mineral dust aerosols based on the brightness temperature difference between infrared channels 8.6  $\mu\text{m}$  and 11  $\mu\text{m}$  as dust often produces stronger absorption at 8.6  $\mu\text{m}$  than that at 11  $\mu\text{m}$  providing a robust way to detect strongly absorbing dust such as the silicates (Hsu *et al.*, 2013). Cloudy pixels are screened by examining the spatial variations of TOA reflectance at 412 nm, 1380 nm, and brightness temperatures in the 11  $\mu\text{m}$  and 12  $\mu\text{m}$  bands. DB performs retrievals on cloud-free and snow-free pixels at nominal 1x1 km spatial resolution, and then aggregates afterward to the 10x10 km retrieval box. Unlike the DT algorithm, DB provides prognostic uncertainty defined relative to DB-retrieved AOT rather than to AERONET AOT. The uncertainty estimates for the best quality retrievals (QAC=3) is formalized as  $\pm ([0.086+0.56\tau_{\text{DB}}] / [1/\mu_0+1/\mu])$ , where  $\tau_{\text{DB}}$  is AOT retrieved by DB algorithm,  $\mu_0$  and  $\mu$  are the cosines of solar and view zenith angles for a given retrieval (Sayer *et al.*, 2013). A detailed description of the second generation, enhanced DB retrieval algorithm is given in Hsu *et al.* (2013).

### 15 **2.3 MODIS Multi-Angle Implementation of Atmospheric Correction Aerosol**

#### **Product**

The Multi-Angle Implementation of Atmospheric Correction (MAIAC) algorithm retrieves surface bi-directional reflection factor (BRF) and AOT by using the time series of MODIS measurements over both dark vegetated surfaces as well as bright targets (Lyapustin *et al.*, 2011). The surface characterization in MAIAC is carried out by deriving the spectral regression coefficients that relate the surface BRF in the blue (470 nm), green (550 nm), and shortwave infrared (2130 nm) bands of MODIS. MAIAC considers two discrete aerosol models, i.e., background and dust for a given location, similar to the ones adopted in MODIS dark target algorithm (Levy *et al.*, 2007). However, MAIAC prescribes 7 different regional aerosol models for different regions of the world and uses either background model or dust model, if the dust aerosols are detected. For identifying the smoke aerosols generated from biomass burning, MAIAC employs a “smoke test” to discriminate smoke from clouds (Lyapustin *et al.*, 2012). The smoke test relies on a relative increase of aerosol absorption at MODIS wavelength 412 nm as compared to 470–670 nm owing to multiple scattering and enhanced absorption by organic carbon released during biomass burning combustion. Each valid 1-km AOT retrieval of MAIAC

is accompanied by the associated quality flags which describe the observed conditions. Since its introduction in 2011-2012, MAIAC algorithm has been continuously updated and evaluated regarding its accuracy and performance. The MAIAC aerosol dataset used in the present study is derived using the latest Collection 6.0 version of the algorithm documented in *Lyapustin et al.* (2018), for which the AOT accuracy can be evaluated as  $\pm(0.05+15\%)*AOT$  or even better  $\pm(0.05+10\%)*AOT$  as shown in a global validation analysis. For a more detailed description of the MAIAC collection 6 algorithm, the reader is referred to *Lyapustin et al.* (2018).

## 2.4 Ground-based AERONET AOT Measurements

The Aerosol Robotic Network (AERONET) project is a ground-based federated network of globally distributed Cimel Sun photometers designed to measure aerosol optical and microphysical properties (*Holben et al.*, 1998). Started in 1992, AERONET has expanded its network from a few sites in the early years to more than 500 sites across the globe currently. For more than 25 years, the project has provided long-term, continuous, and readily accessible public domain database of aerosol optical and microphysical properties. AERONET data has been extensively used for aerosol characterization and validation of satellite retrievals. Spectral AOTs from the direct Sun measurements are available nominally at 340, 380, 440, 500, 675, 870, and 1020 nm. In the present analysis, we employ AERONET Version 2, Level 2 (cloud-cleared and quality-assured) (*Holben et al.*, 2006) spectral AOT dataset from a total of 171 sites span across the United States and Canada. Figure 1 displays the geographical distribution of AERONET sites with the corresponding temporal record (color-coded). Table 1 summarizes the datasets and their characteristics.

## 2.5 Satellite-ground Collocation Strategy

The three MODIS aerosol algorithms report AOT at different spatial resolutions. The DT algorithm performs and reports AOT at 10 km and 3 km spatial resolution; DB performs retrievals at 1 km but aggregates afterward to the 10x10 km retrieval box, whereas the MAIAC algorithm retrieves and reports AOT at a much higher resolution of 1 km. While all three aerosol products report AOT at their respective nadir spatial resolutions, i.e., 10 km and 3 km for DT, 10 km for DB, and 1 km for MAIAC, representing the atmospheric conditions over the respective area intercepted at the ground, the direct measurements of the spectral AOT from AERONET sunphotometer are columnar point measurements. Furthermore, AERONET makes AOT

measurements at an interval of 15 minutes, and the timings of Aqua/MODIS overpass may not closely match with that of AERONET measurements. Therefore, collocating both types of measurements requires a spatiotemporal window that can adequately match the spatially-averaged satellite AOT retrievals with the temporally-averaged ground-based measurements. The spatiotemporal approach developed by *Ichoku et al. (2002)* has been adopted in several validation studies for validating MODIS aerosol products against ground truth, such as from AERONET. The standard approach suggests comparing spatially averaged satellite retrievals in a  $0.5^\circ \times 0.5^\circ$  grid box centered at the ground site with the temporal averaged sunphotometer measurements of AOT within a time window of  $\pm 30$  minutes of satellite overpass time.

10

In this study, we introduce variations in the standard spatiotemporal window by modifying the extent of both spatial and temporal domains to assess the performance of MODIS aerosol products on different space-time scales. Four different spatiotemporal windows were formulated that differ in the size of grid box centered at the AERONET site and corresponding time window around Aqua overpass time for averaging the AERONET AOTs. For the MAIAC and DB products, the minimum number of 1-km satellite observations used by the respective algorithms in the aerosol retrieval is required to be set at 20% of the maximum possible 1-km pixels contained in the respective grid boxes. Since the DT algorithm discards 50% brightest and 20% darkest pixels out of a total number of available 500-meter pixels in each 10 km and 3 km grid box before performing the retrieval, the threshold for DT algorithm was set to 10%. The minimum number of AERONET Level 2 AOTs around the satellite overpass time is required to be at least two for all four variants of the collocation scheme. Table 2 lists the configurations of all four spatiotemporal windows designed for the satellite-ground collocation.

15

20

25

The wavelengths of AOT retrievals differ among the three MODIS aerosol algorithms. While the DT algorithm retrieves and reports AOT at 470, 660, and 2130 nm, DB retrievals are available at 412, 470, and 660 nm. MAIAC retrieves AOT at 470 nm and reports it at 550 nm. For a consistent comparison against AERONET, we choose 470 nm as a reference wavelength since all three algorithms actually retrieve AOT at this common wavelength. AERONET Sunphotometer, on the other hand, does not directly measure AOT at 470 nm but provides measurements at nearby wavelengths, i.e., 440 nm, 500 nm, and 670 nm. Using the Angstrom



Exponent calculated from AOTs at these wavelengths, the AERONET AOT was estimated for the 470 nm wavelength following a linear regression on the AOT versus wavelength relation on a log-log space. The MODIS AOT retrievals at 470 nm were then directly compared against the interpolated AOTs of AERONET at the same wavelength. We use the best quality AOT retrievals as identified in their respective quality assurance fields (i.e., QAC=2 and 3 for DT and DB) of all three aerosol products that are claimed to be higher in confidence and free of cloud contamination.

### 3. Results

#### 3.1 MODIS versus AERONET AOTs: Individual Sites

Figure 2 shows scatter plots of MODIS versus AERONET AOT matchups for the selected individual sites located in Eastern NA. These sites are characterized by lower surface albedo during the spring and summer seasons due to increased green cover, and typically influenced by background and urban-industrial aerosols. Different color codes are used to display matchup points derived following the different collocation approaches described in the previous section. Each AOT dataset was co-located to AERONET independently. While the AOT retrievals from all three algorithms are generally well-correlated ( $R \sim 0.90$ ) with those of AERONET, MAIAC AOTs are found to be slightly under-estimated, albeit with the lowest RMSE and the largest number of matchups among the three algorithms. The performance of DB algorithm is found to be intermediate with relatively better statistics of the comparison than those of DT over sites *CCNY*, *Toronto*, and *Walker\_Branch*, but inferior performance over sites *GSFC* and *Univ\_Of\_Houston*. Table 3 lists various statistical measures of MODIS-AERONET AOT matchups for a number of sites located in Eastern NA.

Figure 3 shows similar MODIS versus AERONET comparison, but for a subset of sites over the western NA characterized by bright surfaces and inhomogeneous surface elevation. The retrieved AOT by the three MODIS algorithms differs markedly over these sites. The DT algorithm, which is designed to produce accurate aerosol retrievals over dark surfaces, significantly overestimates AOTs particularly at a smaller spatial scale of the collocation domain. Noticeably, spatial averaging of DT AOTs over a larger spatial scale ( $40 \times 40 \text{ km}^2$ ) at the *Fresno* site provides

significantly improved agreement with AERONET AOTs as reflected by the different measures of statistics included in the scatter plot. DB and AERONET AOT matchups over these sites are found to be less correlated but with reduced RMSE. Over the *Railroad\_Valley* site, most AOT matchups from DB under all four collocation approaches remained in the range 0.0-0.2, whereas AERONET AOTs varied in the range 0.0-0.4. The MAIAC-AERONET comparison over these sites shows relatively better statistics than those of DT and DB comparisons with a significantly larger number of matchups, higher correlation coefficient, and lower RMSE values. Various statistical measures of MODIS versus AERONET AOT matchups for selected western NA sites are listed in Table 3.

### 3.2 MODIS versus AERONET AOTs: Composites for Eastern and Western North America

This section describes the MODIS-AERONET comparison results obtained by accumulating matchups derived separately for all Eastern and Western NA sites. The top panel of Figure 4 shows the composite comparison of MODIS AOTs to those of AERONET for all Eastern NA sites combined. The comparison includes matchups obtained following the collocation scheme that averages satellite data in  $40 \times 40 \text{ km}^2$  spatial domain and AERONET data within  $\pm 30$  minutes of Aqua overpass time. Satellite-ground matchup points are color-coded according to the density of data for each AOT bin of size 0.01 as depicted in the color bar. One of the striking features of the comparison is that the total number of MAIAC AOT data points collocated with AERONET is significantly larger than those obtained from DB and DT (10-km and 3-km) comparisons. Quantitatively, MAIAC provides  $\sim 115\%$  and  $120\%$  ( $86\%$ ) more matchups than DB 10-km and DT 10-km (3-km aerosol product) products, respectively. In addition to the higher frequency of AOT retrievals, MAIAC AOTs are found to compare better with those of AERONET with an overall lower RMSE (0.056) and a higher correlation ( $R=0.93$ ). Conversely, the performance of the DT 10-km algorithm is relatively inferior in terms of number of matchup points, larger RMSE and bias with the slope (1.23) of the satellite-ground relationship higher than unity. DB and MAIAC comparisons to AERONET provide slopes (0.80 and 0.86) less than 1.0 mainly due to under-estimation (over-estimation) of retrievals at higher (lower) AOTs, but with an overall improvement in the other statistical measures. Noticeably, the DT 3-km product owing to its higher spatial resolution offered more matchups accompanied with similar

correlation ( $\sim 0.93$ ), slope (1.20), and marginally improved RMSE ( $\sim 0.08$ ) compared to those of the 10-km product.

For the combined western NA sites comparison, MAIAC again provides a significantly larger number of matchup points, quantitatively  $\sim 150\%$ ,  $220\%$ , and  $197\%$  compared to DB 10-km, DT 10-km, and DT 3-km products, respectively, with relatively lowest RMSE (0.062) and the highest correlation (0.83). However, the slope of the satellite-ground AOT relationship is found to be the lowest (0.705) for MAIAC results compared to those obtained from DB (0.86), DT 10-km (1.14) and DT 3-km (1.05) datasets. The intercepts of the relationships are found to be comparable for DT and DB ( $\sim 0.02$ ), but higher (0.043) for MAIAC.

The results presented so far considered satellite-ground matchups obtained independently for each MODIS aerosol product. Such comparison allows evaluation of both the relative accuracy of different products as well as the frequency of the retrievals, whereas the comparison imposed by the requirement of having AOT retrievals from all three algorithms simultaneously would provide only the relative accuracy assessment. Such comparison is shown in Figure 5 for eastern (top) and western (bottom) NA sites. Note that the number of matchups is identical for all three algorithms and is drastically lower than the collocation points obtained when matched with AERONET independently. Given the simultaneous measurements of AOT and near-equal sampling among the three algorithms, MAIAC provides highest correlation (0.9 and 0.84) and lowest RMSE (0.053 and 0.052) over eastern and western NA sites, respectively. The slope of the satellite-ground relationship, however, was farthest from unity for MAIAC compared to those of DT and DB results.

### **3.3 Impact of Surface Reflectance on AOT Retrievals**

The surface characterization is a crucial step for delineating surface contribution from the TOA reflectance measurements to separate atmospheric signal for the aerosol retrieval. Earlier studies suggest that an absolute uncertainty of 0.01 in the estimation of surface reflectance in the visible channels can produce an error of up to 0.1, i.e., approximately ten times, in the AOT retrieval from satellites (*Kaufman et al.*, 1997; *Jethva et al.*, 2010). The three independent MODIS aerosol algorithms under consideration here employ different approaches to characterize the surface reflectance as briefly described in the data section. The DT algorithm estimates surface reflectance in the visible channels (470 and 660 nm) through a quasi-static regression between

the reflectance at 2130 nm and those of visible channels by accounting for the dependence of these relationships on scattering angle and NDVI. The surface characterization in the DB algorithm is achieved through a hybrid scheme that applies the dynamical surface reflectance method for urban built-up and the precalculated surface reflectance database in arid and semi-arid areas. The MAIAC algorithm, on the other hand, derives the spectral regression coefficients dynamically that relate the surface reflectance in the 470 nm, 550 nm, and 2130 nm bands of MODIS.

In this section, we explore the relationship between the surface reflectance either assumed (DT and DB) or retrieved (MAIAC) and its impact on the accuracy of AOT retrieved from three algorithms. For this purpose, we consider two datasets: 1) MODIS MYD09 daily L3 Global 0.05Deg CMG atmospheric correction product (Vermote, 2015), and 2) MAIAC BRF retrievals. Both atmospheric correction algorithms differ in their approaches to estimate the surface reflectance by removing scattering and absorption from TOA measurements. Both products dynamically capture the temporal variations of surface properties and provide surface characterization over a wide range of surface conditions, including darker as well as brighter surfaces. The MAIAC BRF product at the time of conducting the present work hasn't been evaluated over the North America region. However, some recent studies have reported a significant increase in the accuracy of MAIAC surface reflectance compared to MODIS standard products MOD09 and MOD035 over tropical Amazon (Hilker et al. 2012; 2014; 2015; Maeda et al., 2016). Furthermore, a study by Chen et al. (2017) found an improvement in leaf area index (LAI) retrievals with the MODIS LAI/FPAR algorithm when using MAIAC instead of standard MODIS MOD09 input. Note that the sole purpose of using the MAIAC surface retrieval dataset here is to evaluate relative differences between satellite retrievals and ground measurements of AOT at varying surface brightness, which in no way constitutes a validation exercise of MAIAC surface retrievals over the study region nor it acts as a bias towards a particular algorithm.

Figure 6 shows box and whisker plots of differences in the AOT (470 nm) between the collocated MODIS retrievals and AERONET measurements as a function of coincident MYD09 BRF for eastern NA sites (top panel) and western NA sites (bottom panel). The collocated dataset of MODIS and AERONET within 40 km diameter centered at AERONET site and  $\pm 30$

minutes of MODIS overpass was used in these calculations. The total number of samples obtained in each bin of surface BRF is depicted at the top of each sub-plot. For the eastern NA sites, the mean and mode of error in DT and DB retrievals show negligible dependence on surface BRF with most matchups remaining close to the no-error limit but with an increased spread in data at surface BRF > 0.06. The error in MAIAC AOT retrievals, however, is found to be very small with the mean and mode for each bin close to no error throughout the entire range of MYD09 BRF retrieved over eastern NA. Also, the spread of error (10 to 90 percentile group) in the MAIAC-AERONET matchups is noted smaller with an error limit mostly confined to within  $\pm 0.1$ .

For the sites located in western NA, the error in DT-retrieved AOT (both 10-km and 3-km) exhibits a systematic behavior showing significant growth of error accompanied by the larger spread in the data population at relatively higher surface BRF (0.05-0.1). Also, note that no sufficient matchups are found between DT and AERONET for conditions when MYD09 retrieved much higher values of surface BRF. Similar results are obtained when MAIAC BRF is used in the analysis shown in Supplementary Figure 1. Both MYD09 and MAIAC BRF datasets, though derived differently, show consistent AOT error characterization as a function of surface reflectance over eastern and western NA region. *Superczynski et al. (2017)* further supports our findings using the AOT validation results of the Suomi-NPP Visible Infrared Imaging Radiometer Suite (VIIRS) aerosol algorithm essentially basing on the DT approach, where VIIRS-derived AOTs are found to be bias significantly higher w.r.t to AERONET measurements over North America at larger values of coincident MAIAC-retrieved surface reflectance. The poor performance of the DT algorithm over brighter surfaces has been a known problem (*Levy et al., 2010*), although it was expected that the DT collection 006 algorithm would yield a lower bias over bright surfaces (*Levy et al., 2013*). The DT algorithm was primarily designed and developed for the aerosol retrieval over darker vegetated surfaces, as the name suggests, and follows the principle that aerosols brighten the scene, which over the brighter surfaces, breaks down. Moreover, aerosol loading over western NA is relatively low, resulting in an inferior signal from aerosols compared to that from a brighter background.

## 4. Concluding Remarks

In this paper, we have performed the accuracy assessment of three Aqua/MODIS products of aerosol optical thickness derived from three independent algorithms using ground-based AERONET measurements over the North America region. This is, to our knowledge, the first attempt to simultaneously evaluate the relative performance of the three MODIS aerosol products, i.e., DT, BB, and MAIAC, over the region, which is in the field-of-view of currently operational GOES geostationary platform and future TEMPO mission. A spatio-temporal collocation scheme of satellite retrievals with ground measurements was applied identically to all three satellite-based products, except for the relaxed required minimum number of retrievals for the DT algorithm which discards many sub-kilometer pixels prior to performing the aerosol inversion. The comparison was carried out over a number of AERONET sites situated mostly in the United States, and a few in Canada for the period 2002-2016, and under two sets of configurations, 1) independent comparison against AERONET, and 2) when retrievals from all three algorithms are available simultaneously.

We find that the performance of all three aerosol algorithms, when assessed independently without having the requirement of simultaneous retrievals from all three algorithms, is comparable over darker surfaces of eastern NA with the MAIAC algorithm providing marginally better results with the lowest RMSE (0.056) and comparable correlation ( $\sim 0.90$ ). On the other hand, the DT algorithm yields larger RMSE (0.095), but offer a better correlation of 0.933; the DB algorithm provided worst correlation (0.0756) with an intermediate RMSE of 0.069. The most significant difference in this comparison has been the number of retrievals with MAIAC yielding significantly more matchups with AERONET than the other two algorithms. MAIAC's number of available retrievals is more than double that of the DT and DB products.

Over the western NA, where the surface is characterized by steep changes in topography and brighter surface background, the AOT retrievals from DT algorithm are found to be overestimated compared to that from AERONET with poorer RMSE, correlation, and bias of  $\sim 0.12$ , 0.82, and 0.037 respectively. In comparison, DB and MAIAC both show a relatively robust match with AERONET resulting in an RMSE of  $\sim 0.06$  and correlation of 0.72-0.83. Noticeably, the MAIAC dataset provides the maximum number of matchups ( $N=27653$ )

compared to that of DB (N=11026) and DT (N=8623 for 10-km and N=9299 for 3-km) – a factor of 2.51 and 3.21 (2.97) higher matchup frequency than that of DB and DT, respectively.

5 The error in AOT characterized as a function of MYD09 and MAIAC bi-directional surface reflectance products reflect the ability of DB and MAIAC algorithms to retrieve AOT with practically no bias over a wide range of surface conditions, whereas DT-retrieved AOTs are found to be systematically overestimated at higher values of surface reflectance ( $>0.05$ ). The results reported here represent an objective, unbiased evaluation of the DT, DB, and MAIAC land AOT retrieval algorithms currently applied to MODIS observations. The detailed statistical evaluation of the performance of each of these three algorithms may be used as guidance in the development of inversion schemes to derive aerosol properties from ABI or other MODIS-like sensors. An accurate AOT product from GOES-ABI measurements would fulfill the GEO-CAPE stated need of an aerosol product that can be used for both climate and air quality applications.

10

## **Acknowledgment**

The authors acknowledge the support of the MODIS Adaptive Processing System (MODAPS) SIPS team (<https://earthdata.nasa.gov/about/sips/sips-modaps>) for processing and making the MODIS aerosol data available to the user community. The presented work was carried as an integral part of the GEO-CAPE Aerosol Working Group activities, and the authors thank group members for their valuable suggestions. Acknowledgments are due to the individual MODIS aerosol teams for their feedback on the correct interpretation and use of the data products evaluated in the present paper.



## **Authors' Contributions**

Dr. Jethva, the leading author, conceptualized the study and wrote the paper. He conducted validation analysis of MAIAC aerosol products using ground based AERONET dataset, whereas Yoshida Yasuko (third author) conducted similar analysis for the Dark Target and Deep Blue aerosol products. Dr. Torres (second author) brought his expertise in interpreting the results and helped improving the manuscript writeup.

## **Additional Information**

The author(s) declare no competing interests, financial or non-financial.



## References

- Chen, C., Knyazikhin, Y., Park, T., Yan, K., Lyapustin, A., Wang, Y., Yang, B., and Myneni, R. B.: Prototyping of LAI and FPAR Algorithm with MODIS MultiAngle Implementation of Atmospheric Correction (MAIAC) data, *Remote Sens.*, 9, 370, <https://doi.org/10.3390/rs9040370>, 2017.
- 5 Fishman, J., L. T. Iraci, J. Al-Saadi, K. Chance, F. Chavez, M. Chin, P. Coble, C. Davis, P. M. DiGiacomo, D. Edwards, A. Eldering, J. Goes, J. Herman, C. Hu, D. J. Jacob, C. Jordan, S. R. Kawa, R. Key, X. Liu, S. Lohrenz, A. Mannino, V. Natraj, D. Neil, J. Neu, M. Newchurch, K. Pickering, J. Salisbury, H. Sosik, A. Subramaniam, M. Tzortziou, J. Wang, and M. Wang : The United States' Next Generation of Atmospheric Composition and Coastal Ecosystem Measurements: NASA's Geostationary Coastal and Air Pollution Events (GEO-CAPE) Mission. *Bull. Amer. Meteor. Soc.*, 93, 1547–1566, <https://doi.org/10.1175/BAMS-D-11-00201.1>, 2012.
- 10 Hilker, T., Lyapustin, A. I., Tucker, C. J., Sellers, P. J., Hall, F. G., and Wang, Y.: Remote Sensing of Tropical Ecosystems: Atmospheric Correction and Cloud Masking Matter, *Remote Sens. Environ.*, 127, 370–384, <https://doi.org/10.1016/j.rse.2012.08.035>, 2012.
- 15 Hilker, T., Lyapustin, A. I., Tucker, C. J., Hall, F. G., Myneni, R. B., Wang, Y., Bi, J., de Moura, Y. M., and Sellers, P. J.: Vegetation dynamics and rainfall sensitivity of the Amazon, *P. Natl. Acad. Sci. USA*, 111, 16041–16046, <https://doi.org/10.1073/pnas.1404870111>, 2014.
- Hilker, T., Lyapustin, A. I., Wang, Y., Hall, F. G., Tucker, C. J., and Sellers, P. J.: On the measurability of change in Amazon vegetation from MODIS, *Remote Sens. Environ.*, 166, 233–242, 2015.
- 20 Holben, B. N., T. F. Eck, I. Slutsker, D. Tanré, J. P. Buis, A. Setzer, E. Vermote, J.A. Reagan, Y.J. Kaufman, T. Nakajima, F. Lavenu, I. Jankowiak, and A. Smirnov: AERONET-A Federated Instrument Network and Data Archive for Aerosol Characterization, *Rem. Sens. Env.*, 66(1), 1-16, [http://dx.doi.org/10.1016/S0034-4257\(98\)00031-5](http://dx.doi.org/10.1016/S0034-4257(98)00031-5), 1998.
- 25 Holben, B. N., T. F. Eck, I. Slutsker, A. Smirnov, A Sinyuk, J. Schafer, D. Giles, O. Dubovik: Aeronet's Version 2.0 quality assurance criteria, *Proc. SPIE 6408, Remote Sensing of the Atmosphere and Clouds*, 64080Q, doi:10.1117/12.706524, 2006.
- Hsu, N. C., Si-Chee Tsay, M. D. King, and J. R. Herman: Aerosol properties over bright-reflecting source regions, *IEEE Trans. on Geosci. Rem. Sens.*, 42(3), pp. 557-569, doi: 10.1109/TGRS.2004.824067, 2004.
- 30 Hsu, N. C., M. -J. Jeong, C. Bettenhausen, A. M. Sayer, R. Hansell, C. S. Seftor, J. Huang, and S. -C. Tsay: Enhanced Deep Blue aerosol retrieval algorithm: The second generation, *J. Geophys. Res. Atmos.*, 118, 9296–9315, doi:10.1002/jgrd.50712, 2013.
- Ichoku, C., D. A. Chu, S. Mattoo, Y. J. Kaufman, L. A. Remer, D. Tanré, I. Slutsker, and B. N. Holben: A spatio-temporal approach for global validation and analysis of MODIS aerosol products, *Geophys. Res. Lett.*, 29(12), doi:10.1029/2001GL013206, 2002.
- 35 Jethva, H., S. K. Satheesh, J. Srinivasan, and R. C. Levy: Improved retrieval of aerosol size-resolved properties from Moderate Resolution Imaging Spectroradiometer over India: Role of aerosol model and surface reflectance, *J. Geophys. Res.*, 115(D18213), doi:10.1029/2009JD013218, 2010.

- Kaufman, Y. J., D. Tanre, L. A. Remer, E. F. Vermote, A. Chu, and B. N. Holben: Operational remote sensing of tropospheric aerosol over the land from EOS-Moderate Resolution Imaging Spectroradiometer, *J. Geophys. Res.*, 102 (D14), 17,051-17,067, 1997.
- 5 Levy, R. C., L. A. Remer, and O. Dubovik: Global aerosol optical properties and application to Moderate Resolution Imaging Spectroradiometer aerosol retrieval over land, *J. Geophys. Res.*, 112, D13210, doi:10.1029/2006JD007815, 2007.
- Levy, R. C., Remer, L. A., Kleidman, R. G., Mattoo, S., Ichoku, C., Kahn, R., and Eck, T. F.: Global evaluation of the Collection 5 MODIS dark-target aerosol products over land, *Atmos. Chem. Phys.*, 10, 10399–10420, doi:10.5194/acp-10-10399-2010, 2010.
- 10 Levy, R. C., Mattoo, S., Munchak, L. A., Remer, L. A., Sayer, A. M., Patadia, F., & Hsu, N. C.: The Collection 6 MODIS aerosol products over land and ocean. *Atmospheric Measurement Techniques*, 6, 2989–3034. doi:10.5194/amt-6-2989-2013, 2013.
- Lyapustin, A., Y. Wang, I. Laszlo, R. Kahn, S. Korkin, L. Remer, R. Levy, and J. S. Reid: Multiangle implementation of atmospheric correction (MAIAC): 2. Aerosol algorithm, *J. Geophys. Res.*, 116, D03211, doi:10.1029/2010JD014986, 2011.
- 15 Lyapustin, A., S. Korkin, Y. Wang, B. Quayle, and I. Laszlo: Discrimination of biomass burning smoke and clouds in MAIAC algorithm, *Atmos. Chem. Phys.*, 12(20), 9679–9686, doi:10.5194/acp-12-9679-2012, 2012.
- Lyapustin, A., Y. Wang, S. Korkin, and D. Huang: MODIS Collection 6 MAIAC Algorithm, *Atmos. Meas. Tech.*, 11, 5741-5765, <https://doi.org/10.5194/amt-11-5741-2018>, 2018.
- 20 Maeda, E. E., Moura, M. Y., Wagner, F., Hilker, T., Lyapustin, A. I., Wang, Y., Mõttus, M., Aragão, L. E. O. C., and Shimabukuro, Y.: Consistency of vegetation index seasonality across the Amazon rainforest, *Int. J. Appl. Earth. Obs.*, 52, 42–53, 2016.
- Martins, J. V., D. Tanré, L. Remer, Y. Kaufman, S. Mattoo, and R. Levy: MODIS Cloud screening for remote sensing of aerosols over oceans using spatial variability, *Geophys. Res. Lett.*, 29, 8009, doi:10.1029/2001GL013252, 2002.
- 25 Mhawish, A., M. Sorek-Hamer, T. Banerjee, A. Lyapustin, D. M. Broday, and R. Chatfield (2018), Inter-comparison and evaluation of MODIS C6 MAIAC, DB and DT AOD over South Asia, *Remote Sensing of Environment.*, Submitted.
- 30 Remer, L. A., Y. J. Kaufman, D. Tanré, S. Mattoo, D. A. Chu, J. V. Martins, R. Li, C. Ichoku, R. C. Levy, R. G. Kleidman, T. F. Eck, E. Vermote, and B. N. Holben: The MODIS Aerosol Algorithm, Products, and Validation. *J. Atmos. Sci.*, 62, 947-973, <https://doi.org/10.1175/JAS3385.1>, 2005.
- Remer, L. A., Mattoo, S., Levy, R. C., and Munchak, L. A.: MODIS 3 km aerosol product: algorithm and global perspective, *Atmos. Meas. Tech.*, 6, 1829-1844, <https://doi.org/10.5194/amt-6-1829-2013>, 2013.
- 35 Sayer, A. M., N. C. Hsu, C. Bettenhausen, and M. -J. Jeong: Validation and uncertainty estimates for MODIS Collection 6 “Deep Blue” aerosol data, *J. Geophys. Res. Atmos.*, 118, 7864–7872, doi:10.1002/jgrd.50600, 2013.
- Sayer, A. M., L. A. Munchak, N. C. Hsu, R. C. Levy, C. Bettenhausen, and M.-J. Jeong: MODIS Collection 6 aerosol products: Comparison between Aqua's e-Deep Blue, Dark Target, and “merged” data

sets, and usage recommendations, *J. Geophys. Res. Atmos.*, 119, 13,965-13,989, doi:[10.1002/2014JD022453](https://doi.org/10.1002/2014JD022453), 2014.

- 5 Superczynski, S. D., S. Kondragunta and A. I. Lyapustin: Evaluation of the multi-angle implementation of atmospheric correction (MAIAC) aerosol algorithm through intercomparison with VIIRS aerosol products and AERONET, *J. Geophys. Res. Atmos.*, 122, 3005–3022, doi:[10.1002/2016JD025720](https://doi.org/10.1002/2016JD025720), 2017.
- 10 Zoogman, P., Liu, X., Suleiman, R., Pennington, W., Flittner, D., Al-saadi, J., Hilton, B., Nicks, D., Newchurch, M., Carr, J., Janz, S., Andraschko, M., Arola, A., Baker, B., Canova, B., Chan Miller, C., Cohen, R., Davis, J., Dussault, M., Edwards, D., Fishman, J., Ghulam, A., González Abad, G., Grutter, M., Herman, J., Houck, J., Jacob, D., Joiner, J., Kerridge, B., Kim, J., Krotkov, N., Lamsal, L., Li, C., Lindfors, A., Martin, R., Mcelroy, C., Mclinden, C., Natraj, V., Neil, D., Nowlan, C., O'sullivan, E., Palmer, P., Pierce, R., Pippin, M., Saiz-lopez, A., Spurr, R., Szykman, J., Torres, O., Veefkind, J., Veihelmann, B., Wang, H., Wang, J., and Chance, K.: Tropospheric emissions: Monitoring of pollution (TEMPO), *Journal of quantitative spectroscopy & radiative transfer*, 186, 17-39, doi:[10.1016/j.jqsrt.2016.05.008](https://doi.org/10.1016/j.jqsrt.2016.05.008), 2017.
- 15 Vermote, E. (2015), MOD09A1 MODIS Surface Reflectance 8-Day L3 Global 500m SIN Grid V006. NASA EOSDIS Land Processes DAAC, <http://doi.org/10.5067/MODIS/MYD09A1.006> (Aqua).

# List of Tables

**Table 1.** MODIS-AERONET aerosol datasets and their characteristics.

5 **Table 2.** Configurations of four spatiotemporal windows for the collocation of MODIS and AERONET AOT datasets. Acronyms: DT: Dark Target; DB: Deep Blue; MAIAC: Multi-Angle Implementation of Atmospheric Correction

10 **Table 3.** Statistical measures of MODIS-AERONET AOT (470 nm) matchups for sites in eastern North America. Numbers in bold indicate relatively best performance in respective measures. Abbreviations: Lon.: Longitude, Lat.: Latitude, N: number of satellite-ground matchups, R: correlation, RMSE: root-mean-square-error between MODIS and AERONET, Bias: mean bias, Slope and Intercept: slope and intercept of the linear regression between MODIS and AERONET AOT matchups.

15

**Table 4.** Same as in Table 3 but for sites in western North America.

*Table 1 MODIS-AERONET aerosol datasets and their characteristics.*

Dataset	Characteristics			
	Collection	Data	Product Resolution	In this study
<b>MODIS Dark Target 10-km Aerosol Product MYD04_L2</b>	6.1	Level 2 AOT at 470, 660, and 2100 nm	10 km <sup>2</sup> at nadir	Use of only “good” (QAC=2) and “best” (QAC=3) quality retrievals
<b>MODIS Dark Target 3-km Aerosol Product MYD04_L2</b>	6.1	Level 2 AOT at 470, 660, and 2100 nm	3 km <sup>2</sup> at nadir	Use of only “good” (QAC=2) and “best” (QAC=3) quality retrievals
<b>MODIS Deep Blue Aerosol Product Merged with MYD04_L2</b>	6.1	Level 2 AOT at 412, 470, and 660 nm	10 km <sup>2</sup> at nadir	Use of only “good” (QAC=2) and “best” (QAC=3) quality retrievals
<b>MODIS MAIAC Aerosol Product MCD19A2</b>	6.0	Level 2 Daily L2G 1 km SIN Grid AOT at 470 and 550 nm	1 km <sup>2</sup>	Use of only “good” and “best” quality retrievals
<b>AERONET AOT Product</b>	Level 2.0 Version 2.0	Spectral AOTs	Columnar point measurements	Cloud-cleared and quality assured data

**Table 2 Configurations of four spatiotemporal windows for the collocation of MODIS and AERONET AOT datasets. Acronyms: DT: Dark Target; DB: Deep Blue; MAIAC: Multi-Angle Implementation of Atmospheric Correction**

Grid box size in km <sup>2</sup>	Required minimum number of satellite observations at 1 km in the grid box				$\Delta T$ = Time window between the satellite overpass and AERONET measurements	Minimum number of AERONET Level 2 observations within $\Delta T$
	DT 10-km	DT 3-km	DB	MAIAC		
<b>5</b>	2	5	5	5	$\pm 15$ minutes	2
<b>10</b>	10	20	20	20	$\pm 15$ minutes	2
<b>20</b>	40	80	80	80	$\pm 15$ minutes	2
<b>40</b>	160	320	320	320	$\pm 30$ minutes	2



**Table 3 Statistical measures of MODIS-AERONET AOT (470 nm) matchups for sites in eastern North America. Numbers in bold indicate relatively best performance in respective measures.**

Abbreviations: Lon.: Longitude, Lat.: Latitude, N: number of satellite-ground matchups, R: correlation, RMSE: root-mean-square-error between MODIS and AERONET, Bias: mean bias between the two datasets, Slope and Intercept: slope and intercept of the linear regression between MODIS and AERONET AOT matchups.

5

Sitename	Lon.	Lat.	N	R	RMSE	Bias	Slope	Intercept
Dart Target/Deep Blue/MAIAC								
Ames	-93.78	42.02	427/464/585	<b>0.89/0.89/0.80</b>	0.10/0.08/0.08	-0.04/-0.02/-0.03	1.00/0.84/0.70	-0.04/0.00/0.01
Appalachian_State	-81.69	36.22	352/320/355	<b>0.92/0.91/0.87</b>	0.06/0.05/0.03	<b>-0.01/-0.04/-0.01</b>	1.32/0.67/0.81	-0.04/-0.01/0.01
Billerica	-71.27	42.53	304/283/370	<b>0.96/0.88/0.93</b>	0.07/0.07/0.05	-0.04/0.02/-0.01	1.17/0.79/0.86	-0.07/0.05/0.01
BONDVILLE	-88.37	40.05	539/724/821	<b>0.92/0.91/0.63</b>	0.09/0.05/0.12	-0.04/-0.01/-0.02	1.16/0.89/0.47	-0.07/0.01/0.06
Bratts_Lake	-104.70	50.28	631/528/747	<b>0.94/0.91/0.93</b>	0.16/0.13/0.06	0.11/0.02/0.01	1.50/1.44/1.06	0.04/-0.04/0.01
Brookhaven	-72.89	40.87	154/41/243	<b>0.97/0.97/0.96</b>	0.08/0.06/0.05	0.03/0.02/0.00	1.20/0.87/0.92	<b>-0.01/0.05/0.01</b>
CARTEL	-71.93	45.38	358/420/440	0.91/0.89/0.92	0.07/0.06/0.05	<b>0.00/0.00/-0.03</b>	<b>1.11/0.80/0.83</b>	-0.02/0.03/-0.01
Cart_Site	-97.49	36.61	1339/1235/1685	<b>0.89/0.83/0.82</b>	0.09/0.05/0.05	-0.07/-0.02/-0.01	<b>0.95/0.68/0.74</b>	-0.06/0.01/0.03
CCNY	-73.95	40.82	366/478/730	<b>0.93/0.92/0.91</b>	0.10/0.07/0.06	0.04/0.03/-0.03	1.23/0.98/0.79	-0.01/0.03/0.00
Chapais	-74.98	49.82	168/281/343	<b>0.96/0.90/0.96</b>	0.09/0.08/0.04	0.029/0.00/-0.01	1.27/1.06/0.95	<b>-0.01/-0.01/-0.01</b>
Dayton	-84.11	39.78	205/223/253	<b>0.91/0.89/0.89</b>	0.05/0.04/0.04	<b>0.01/0.01/-0.02</b>	1.23/0.85/0.91	-0.02/0.03/-0.01
Easton_Airport	-76.07	38.81	123/111/224	<b>0.97/0.92/0.92</b>	0.08/0.07/0.05	0.03/0.04/-0.02	1.27/0.94/0.84	-0.02/0.05/0.00
Egbert	-79.75	44.23	681/591/781	<b>0.97/0.96/0.96</b>	0.07/0.07/0.05	<b>0.01/0.03/-0.01</b>	1.24/1.08/1.00	-0.03/0.02/-0.01
Georgia_Tech	-84.40	33.78	306/301/317	<b>0.94/0.88/0.93</b>	0.07/0.05/0.04	-0.05/0.01/0.02	1.26/0.81/0.97	-0.07/0.03/-0.01
GSFC	-76.84	38.99	1188/1182/1336	<b>0.96/0.91/0.94</b>	0.06/0.07/0.04	<b>0.00/0.03/-0.02</b>	1.18/0.79/0.91	-0.03/0.06/-0.01
Halifax	-63.59	44.64	94/147/542	<b>0.94/0.86/0.94</b>	0.06/0.06/0.04	0.04/0.05/0.00	1.30/0.91/0.93	<b>0.00/0.06/0.01</b>
Harvard_Forest	-72.19	42.53	327/338/417	<b>0.96/0.88/0.95</b>	0.06/0.06/0.04	<b>0.01/-0.01/-0.01</b>	1.27/0.89/0.95	-0.03/0.01/-0.01
Howland	-68.73	45.20	157/189/222	<b>0.94/0.89/0.94</b>	0.07/0.06/0.05	<b>0.00/0.00/-0.02</b>	1.20/0.92/0.92	-0.03/0.01/-0.01
Kellogg_LTER	-85.37	42.41	206/214/251	<b>0.95/0.90/0.92</b>	0.07/0.06/0.06	-0.01/0.00/-0.03	1.23/0.88/0.90	-0.05/0.02/-0.02
KONZA_EDC	-96.61	39.10	855/802/1000	0.89/0.90/0.86	0.06/0.04/0.05	-0.02/0.00/-0.01	<b>1.12/0.84/0.80</b>	-0.04/0.02/0.02
MD_Science_Center	-76.62	39.28	633/691/927	<b>0.95/0.88/0.91</b>	0.07/0.06/0.05	-0.02/0.01/0.02	<b>1.14/0.69/0.81</b>	-0.04/0.05/0.00
Pickle_Lake	-90.22	51.45	166/355/430	0.92/0.91/0.93	0.06/0.05/0.05	0.03/-0.01/0.00	1.26/0.95/1.09	<b>0.00/-0.01/-0.01</b>
SERC	-76.50	38.88	471/263/783	<b>0.97/0.95/0.96</b>	0.07/0.05/0.04	<b>0.00/0.03/-0.01</b>	1.23/0.88/0.96	-0.04/0.04/0.00
Sioux_Falls	-96.63	43.74	676/673/822	<b>0.92/0.92/0.89</b>	0.08/0.07/0.06	-0.03/-0.02/-0.01	1.12/1.06/0.81	-0.04/-0.03/0.01
Thompson_Farm	-70.95	43.11	488/435/639	<b>0.94/0.88/0.92</b>	0.06/0.06/0.05	<b>-0.01/0.02/-0.02</b>	1.15/0.83/0.86	-0.03/0.04/0.00
Toronto	-79.47	43.97	474/437/576	<b>0.92/0.91/0.92</b>	0.09/0.06/0.05	0.04/0.02/-0.02	1.23/0.85/0.88	-0.01/0.05/0.00
UAHuntsville	-86.65	34.73	216/194/226	<b>0.97/0.96/0.94</b>	0.06/0.03/0.04	-0.04/-0.01/-0.02	1.31/0.87/0.96	-0.08/0.01/-0.02
UMBC	-76.71	39.26	291/341/401	<b>0.95/0.82/0.90</b>	0.06/0.06/0.05	-0.03/0.02/-0.02	1.23/0.68/0.81	-0.06/0.06/0.01
Univ_of_Houston	-95.34	29.72	418/417/608	<b>0.92/0.69/0.85</b>	<b>0.05/0.1/0.05</b>	<b>0.01/0.07/-0.02</b>	<b>1.22/0.66/0.76</b>	-0.02/0.11/0.01
Walker_Branch	-84.29	35.96	<b>385/354/379</b>	<b>0.97/0.96/0.96</b>	0.08/0.05/0.05	<b>-0.01/-0.02/-0.03</b>	1.30/0.95/0.95	-0.07/-0.01/-0.02
Wallops	-75.48	37.94	398/225/671	0.94/0.95/0.95	0.10/0.08/0.06	0.05/0.04/-0.02	<b>1.08/0.87/0.85</b>	0.03/0.07/0.00

**Table 4 Same as in Table 3 but for sites in western North America.**

Sitename	Long.	Lat.	N	R	RMSE	Bias	Slope	Intercept
<i>Bozeman</i>	-111.05	45.66	719/486/794	0.97/0.95/0.94	0.07/0.06/0.06	0.04/-0.03/0.01	1.05/0.90/0.78	0.04/-0.02/0.04
<i>BSRN_BAO_Boulder</i>	-105.01	40.05	967/828/1421	0.87/0.73/0.81	0.08/0.07/0.05	0.05/-0.05/0.01	1.28/0.43/0.87	0.02/0.01/0.03
<i>CalTech</i>	-118.13	34.14	590/556/698	0.71/0.53/0.79	0.13/0.08/0.06	0.09/-0.01/-0.03	1.05/0.39/0.58	0.08/0.08/0.03
<i>El_Segundo</i>	-118.38	33.91	313/160/826	0.60/0.60/0.72	0.30/0.15/0.05	0.25/0.13/0.01	1.79/0.96/0.71	0.16/0.13/0.04
<i>Frenchman_Flat</i>	-115.94	36.81	137/695/917	0.51/0.47/0.64	0.27/0.06/0.05	0.25/0.01/0.02	1.86/0.50/0.67	0.20/0.05/0.05
<i>Fresno_2</i>	-119.77	36.79	664/733/759	0.77/0.79/0.82	0.08/0.07/0.05	0.02/0.04/-0.01	1.00/0.85/0.74	0.02/0.06/0.02
<i>Fresno</i>	-119.77	36.78	1065/1108/1141	0.72/0.82/0.79	0.07/0.06/0.07	0.01/0.01/-0.03	0.78/0.74/0.57	0.04/0.06/0.04
<i>Goldstone</i>	-116.79	35.23	85/639/1081	0.55/0.49/0.69	0.24/0.06/0.06	0.23/0.03/0.05	1.73/0.72/0.80	0.19/0.04/0.06
<i>Hermosillo</i>	-110.96	29.08	111/321/374	0.83/0.68/0.67	0.05/0.06/0.05	0.03/-0.05/0.00	1.16/0.55/0.70	0.01/0.00/0.04
<i>HJAndrews</i>	-122.22	44.24	743/716/786	0.89/0.88/0.91	0.06/0.07/0.04	0.03/-0.04/0.01	0.98/1.02/0.88	0.03/-0.04/0.02
<i>Kelowna</i>	-119.37	49.96	287/221/350	0.93/0.85/0.93	0.06/0.09/0.04	-0.01/-0.02/0.00	1.10/1.14/0.91	-0.02/0.03/0.01
<i>Kelowna_UAS</i>	-119.40	49.94	599/457/756	0.95/0.84/0.70	0.06/0.08/0.15	0.00/-0.02/-0.01	1.12/1.09/0.38	-0.02/-0.03/0.07
<i>Kirtland_AFB</i>	-106.51	34.95	123/187/274	0.62/0.43/0.80	0.08/0.03/0.04	0.06/-0.02/0.03	1.24/0.11/1.17	0.05/0.02/0.02
<i>La_Jolla</i>	-117.25	32.87	292/115/800	0.73/0.68/0.80	0.06/0.05/0.09	0.00/0.01/0.00	0.95/0.41/0.43	0.00/0.06/0.06
<i>Maricopa</i>	-111.97	33.07	48/744/890	0.81/0.46/0.69	0.13/0.06/0.05	0.13/-0.03/0.03	1.56/0.42/0.76	0.07/0.03/0.05
<i>Missoula</i>	-114.08	46.92	771/653/924	0.96/0.90/0.94	0.06/0.13/0.1	0.00/-0.04/-0.02	1.08/1.21/0.71	-0.01/-0.07/0.03
<i>Monterey</i>	-121.86	36.59	932/545/1306	0.88/0.69/0.86	0.08/0.13/0.11	-0.02/0.05/0.01	1.14/0.81/0.68	-0.04/0.07/0.05
<i>NASA_Ames</i>	-122.06	37.42	136/112/170	0.67/0.77/0.86	0.07/0.06/0.03	0.03/0.04/0.02	1.16/0.81/0.85	0.01/0.06/0.03
<i>NEON-Boulder</i>	-105.27	40.01	55/41/71	0.90/0.82/0.89	0.07/0.04/0.04	0.04/-0.03/0.02	1.32/0.37/0.97	0.01/0.02/0.02
<i>NEON_CVALLA</i>	-105.17	40.16	314/256/415	0.92/0.71/0.87	0.08/0.09/0.05	0.03/-0.03/0.02	1.31/0.99/0.87	0.00/-0.03/0.03
<i>Railroad_Valley</i>	-115.96	38.50	134/558/1718	0.55/0.68/0.74	0.25/0.06/0.05	0.23/-0.02/0.03	1.50/0.26/0.71	0.20/0.02/0.05
<i>Red_Mountain_Pass</i>	-107.73	37.91	113/51/195	0.80/0.38/0.63	0.05/0.03/0.04	0.04/-0.01/0.03	1.10/0.13/0.76	0.03/0.03/0.04
<i>Rimrock</i>	-116.99	46.49	922/826/1167	0.90/0.89/0.90	0.17/0.15/0.09	0.07/0.01/0.03	1.84/1.32/0.80	-0.03/-0.03/0.06
<i>Rogers_Dry_Lake</i>	-117.89	34.93	24/325/472	0.40/0.50/0.64	0.16/0.09/0.06	0.15/0.05/0.03	1.39/0.74/0.58	0.13/0.07/0.06
<i>Sandia_NM_PSEL</i>	-106.54	35.06	182/237/430	0.62/0.45/0.72	0.11/0.04/0.06	0.07/-0.02/0.04	1.40/0.1/1.0	0.05/0.02/0.04
<i>Sevilleta</i>	-106.89	34.36	441/1031/1462	0.63/0.61/0.76	0.16/0.05/0.05	0.14/-0.03/0.03	1.81/0.22/0.82	0.1/0.02/0.04
<i>TABLE_MOUNTAIN_CA</i>	-117.68	34.38	1108/1171/1532	0.64/0.44/0.69	0.14/0.06/0.06	0.12/0.04/0.05	1.59/0.73/0.87	0.09/0.05/0.05
<i>Table_Mountain</i>	-105.24	40.13	519/443/686	0.91/0.89/0.88	0.07/0.06/0.05	0.03/-0.03/0.02	1.20/0.67/0.84	0.01/0.00/0.00
<i>Trinidad_Head</i>	-124.15	41.05	355/166/746	0.84/0.80/0.87	0.09/0.10/0.07	0.02/-0.01/0.00	0.96/0.72/0.72	0.03/0.02/0.03
<i>Tucson</i>	-110.95	32.23	310/454/595	0.59/0.43/0.60	0.19/0.05/0.05	0.17/-0.01/0.03	1.61/0.30/0.65	0.12/0.04/0.06
<i>UCLA</i>	-118.45	34.07	215/174/261	0.62/0.43/0.81	0.12/0.09/0.06	0.06/0.01/-0.04	0.91/0.39/0.62	0.08/0.10/0.02
<i>UCSB</i>	-119.85	34.42	927/540/1184	0.80/0.71/0.90	0.07/0.06/0.05	-0.05/-0.02/-0.02	0.77/0.52/0.71	-0.02/0.04/0.01
<i>Univ_of_Lethbridge</i>	-112.87	49.68	395/312/522	0.97/0.94/0.93	0.14/0.11/0.06	0.09/0.01/0.02	1.52/1.39/0.80	0.03/-0.03/0.04
<i>White_Sands_HELSTF</i>	-106.34	32.64	329/672/1306	0.78/0.59/0.70	0.17/0.05/0.06	0.16/-0.01/0.05	1.45/0.58/0.86	0.13/0.01/0.05

## List of Figures

- 5 **Figure 1** a) Geographical distribution of AERONET sites over North America. Color codes represent the span of AERONET Level 2 data in years calculated from the total number of daily observations. b) An illustration of the spatiotemporal schemes for collocating the satellite retrievals with the ground measurements.
- 10 **Figure 2** Scatterplots comparing the aerosol optical thickness (470 nm) retrieved from the three standard aerosol algorithms of MODIS against that of AERONET for selected sites over eastern, central, and southern N. A. Statistical measures of the comparison are depicted within each plot with different color codes denoting matchups obtained following the four spatiotemporal schemes, i.e., black, blue, green, and red for 5 km, 10 km, 20 km, and 40 km grid boxes.
- Figure 3** Same as in Figure 3 but for AERONET sites located in the western N. A.
- 15 **Figure 4** Scatterplots comparing MODIS-AERONET AOT matchups for all sites combinedly located in eastern N. A. (top panel) and western N. A. (bottom panel). MODIS-AERONET matchups derived independently without the requirement of having simultaneous measurements. The color codes denote the number density of matchups for each bin of AOT.
- 20 **Figure 5** Scatterplots comparing MODIS-AERONET AOT matchups obtained over all sites located in eastern N. A. (top panel) and western N. A. (bottom panel). Only those satellite-ground matchups were included for which AOT retrievals/measurements from all four methods are available simultaneously. The color codes denote the number density of matchups for each bin of AOT.
- 25 **Figure 6** Difference in AOT (470 nm) between MODIS and AERONET as a function of coincident bi-directional reflectance retrievals (470 nm) from MODIS-MOD09 product for eastern NA (a, top) and western NA (b, bottom). Data are represented as a box-and-whisker plot with the thick horizontal line as the median, black dot as mean, shaded boxes are covering 75 and 25 percentiles, and vertical lines as 1.5 times the interquartile range (25-75 percentile). The number of matchups for each bin is given at the top of the plot.
- 30

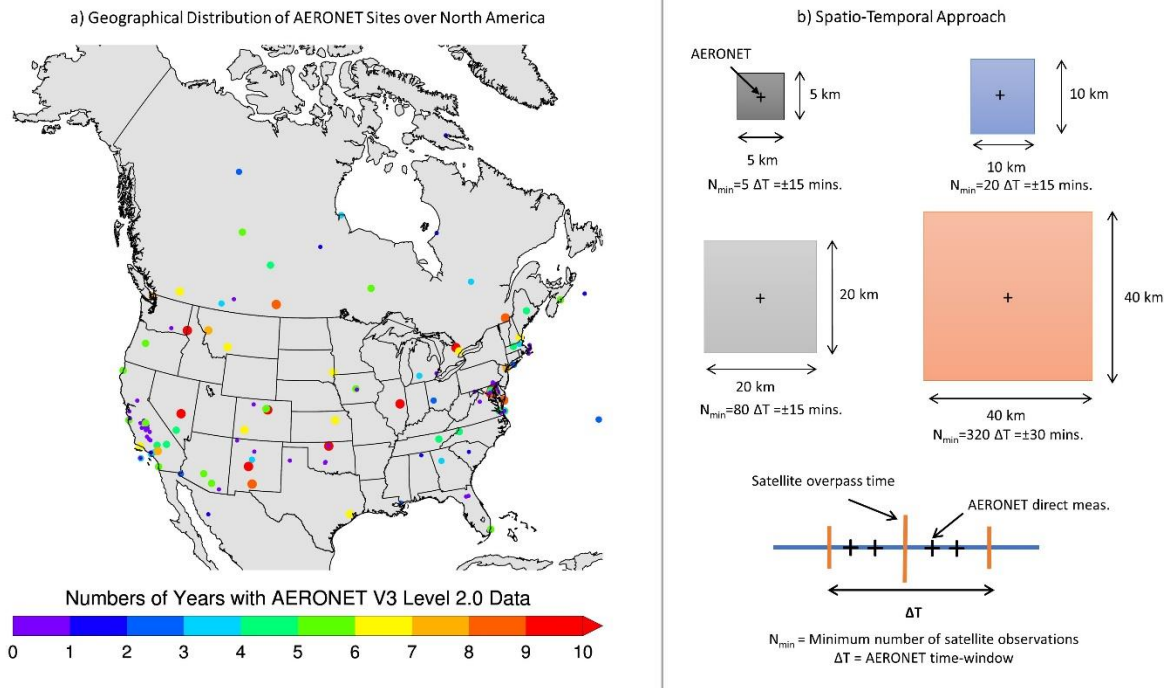


**Figure 1** a) Geographical distribution of AERONET sites over North America. Color codes represent the span of AERONET Version 3 Level 2 data in years calculated from the total number of daily observations. b) An illustration of the spatiotemporal schemes for collocating the satellite retrievals with the ground measurements.

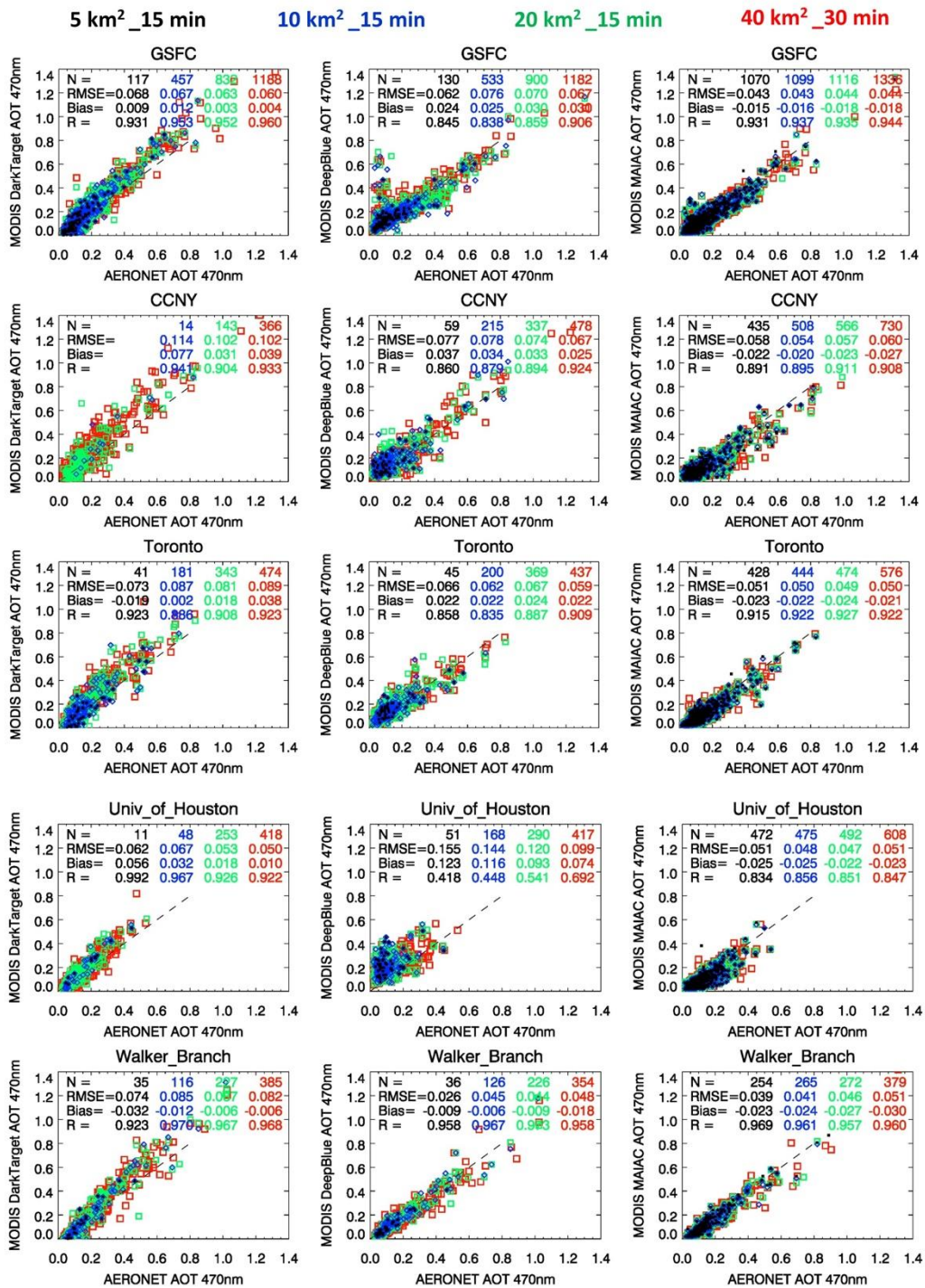


**Figure 2** Scatterplots comparing the aerosol optical thickness (470 nm) retrieved from the three standard aerosol algorithms of MODIS against that of AERONET for selected sites over eastern, central, and southern N. A. Statistical measures of the comparison are depicted within each plot with different color codes denoting matchups obtained following the four spatiotemporal schemes, i.e., black, blue, green, and red for 5 km, 10 km, 20 km, and 40 km grid boxes.

5



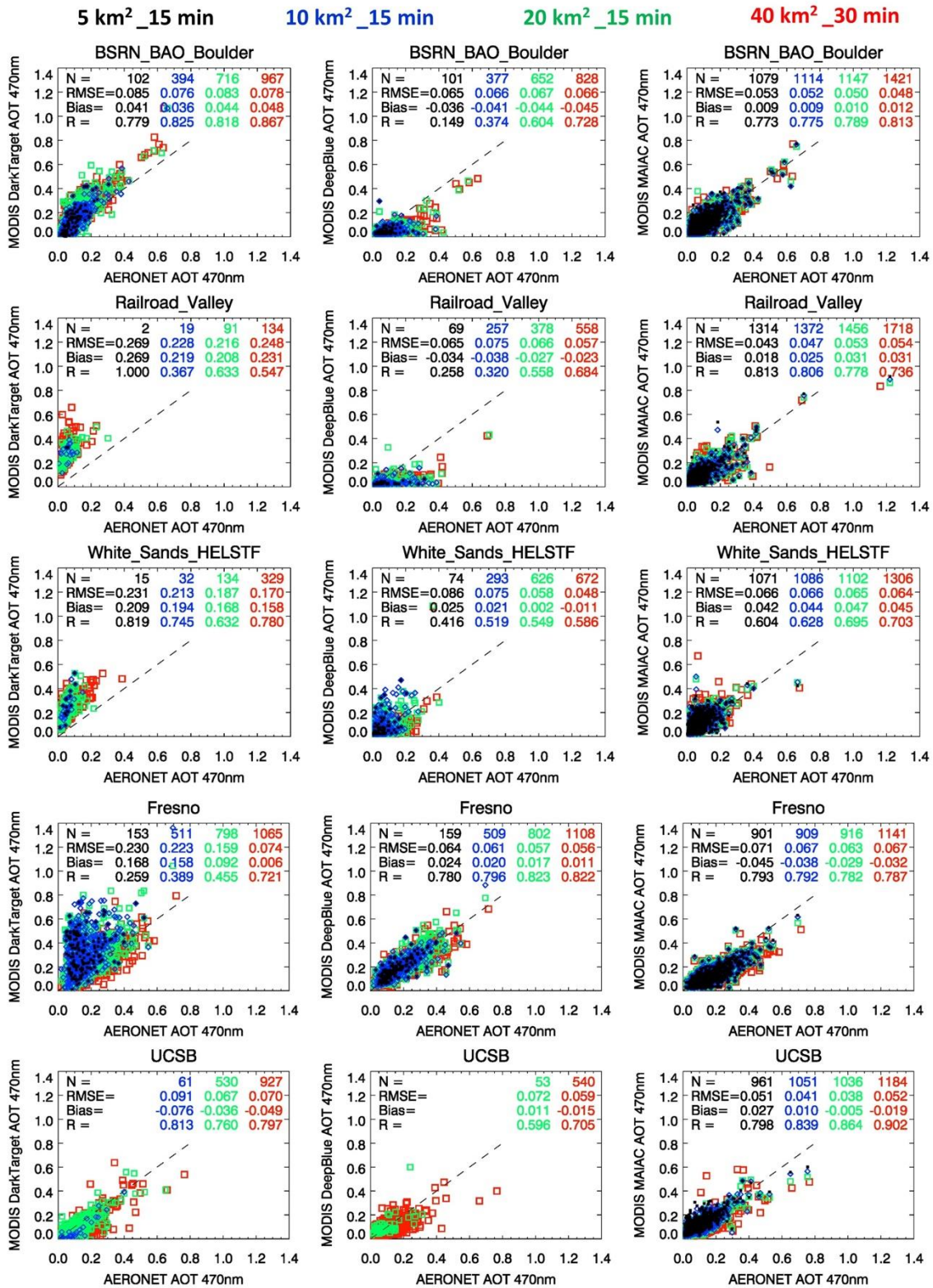
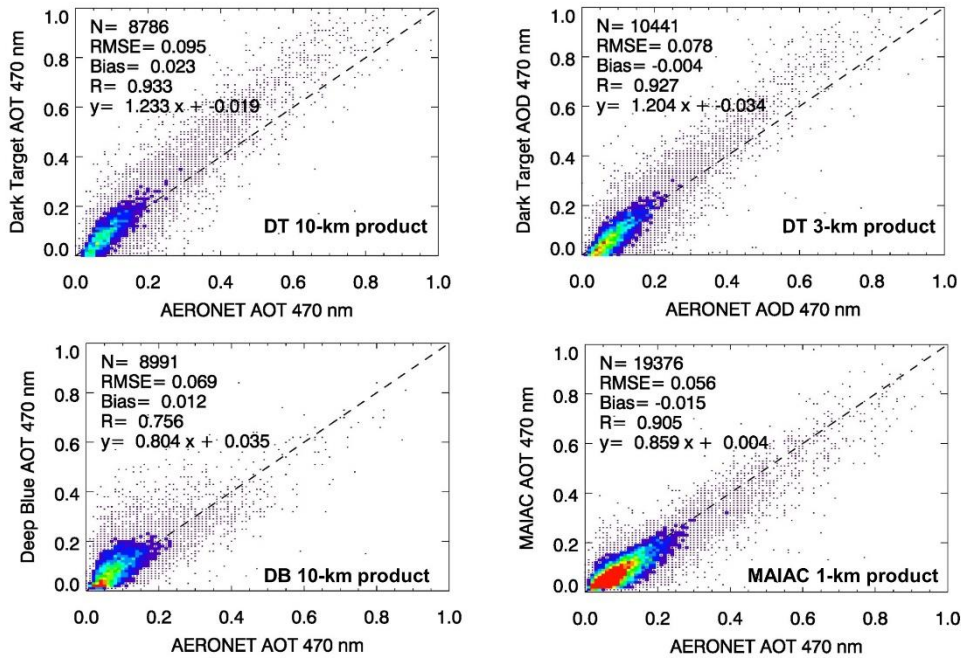


**Figure 3** As in Figure 2 but for AERONET sites located in the western N. A.

40 km<sup>2</sup>\_30 min

a) Eastern North America Sites



b) Western North America Sites

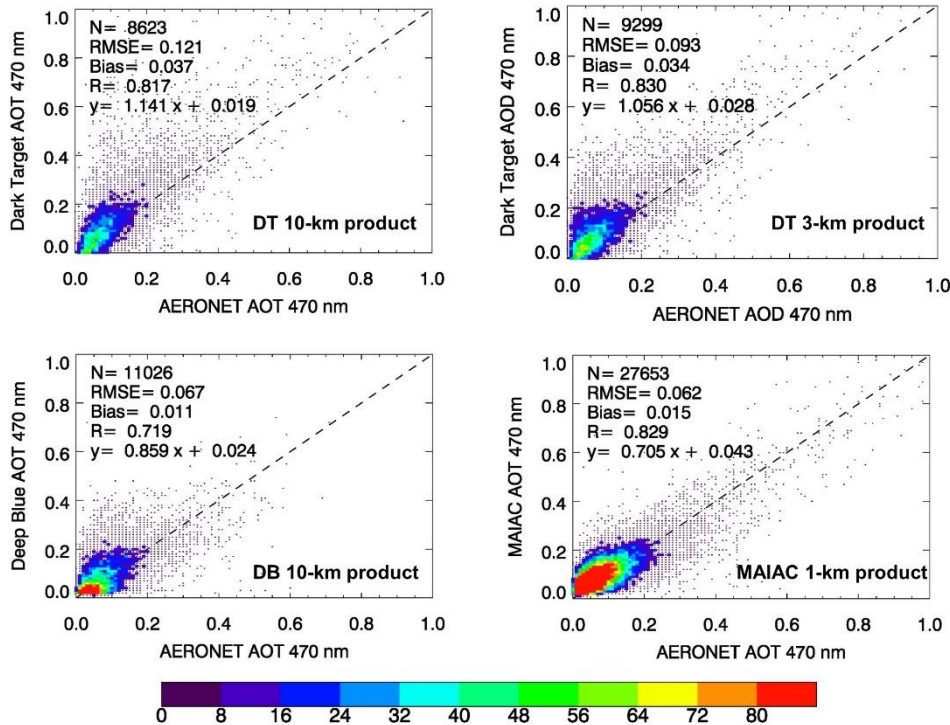


**Figure 4** Scatterplots comparing MODIS-AERONET AOT matchups obtained over all sites located in eastern N. A. (top panel) and western N. A. (bottom panel). MODIS-AERONET matchups derived independently without the requirement of having simultaneous measurements. The color codes denote the number density of matchups for each bin of AOT.

5

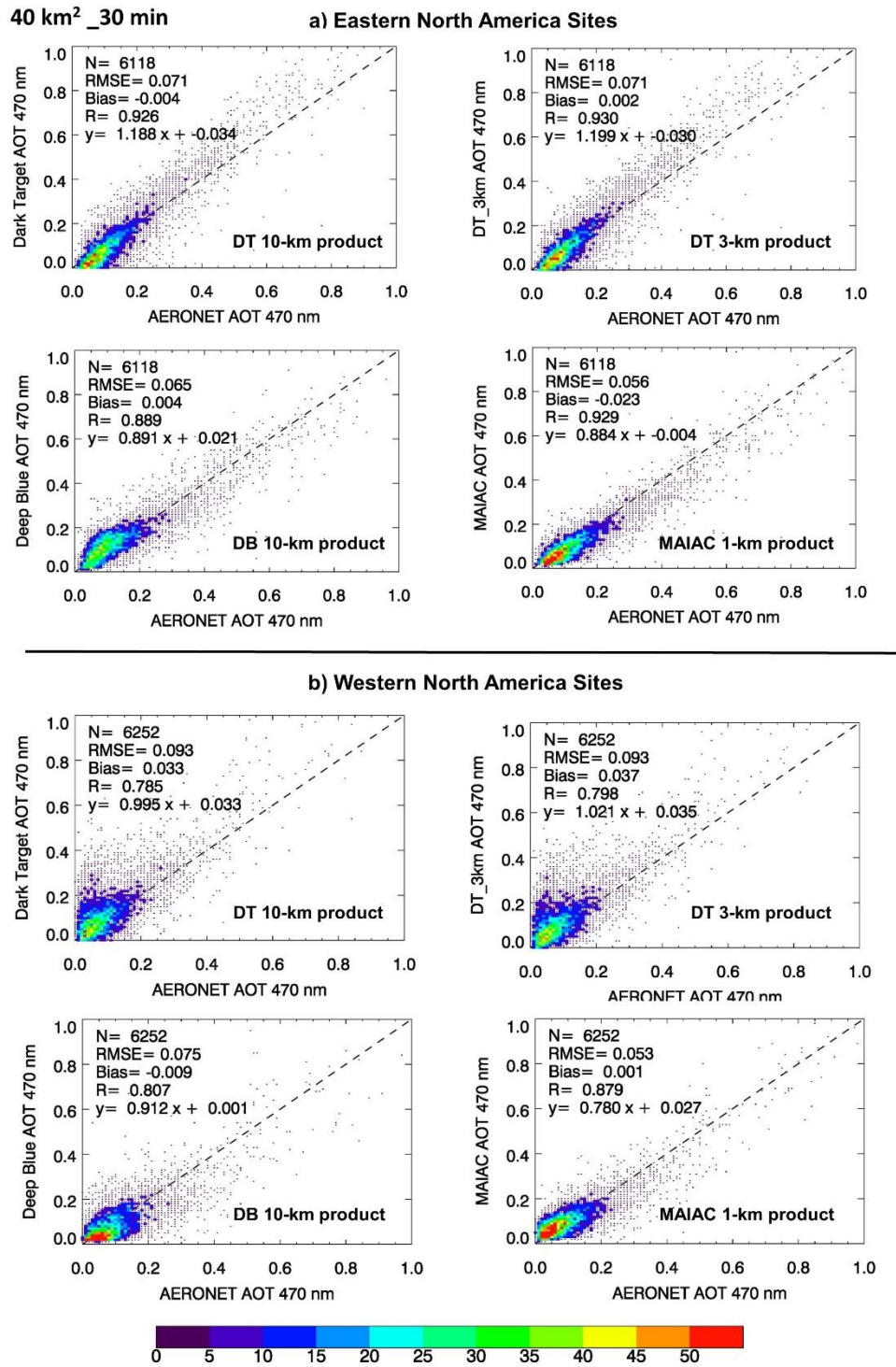
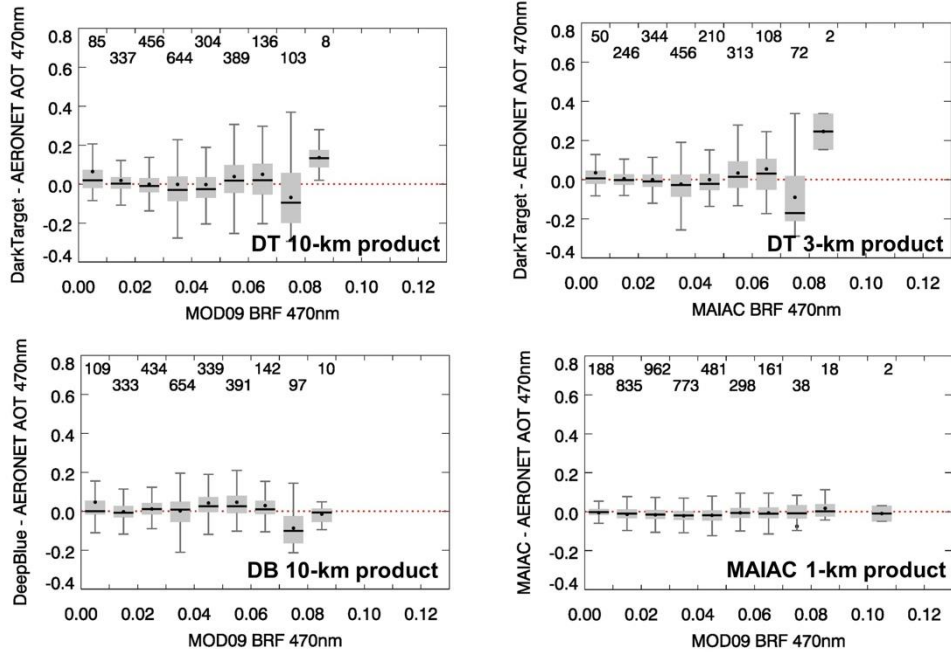


**Figure 5** Scatterplots comparing MODIS-AERONET AOT matchups obtained over all sites located in eastern NA (top panel) and western NA (bottom panel). Only those satellite-ground matchups were included for which AOT retrievals/measurements from all four methods are available simultaneously. The color codes denote the number density of matchups for each bin of AOT.

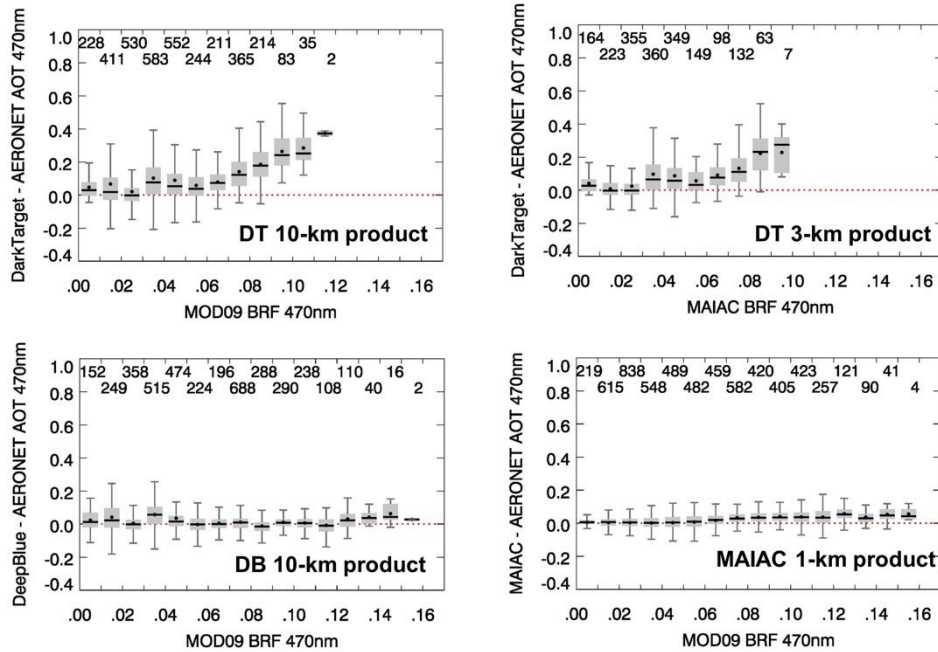


40 km<sup>2</sup> \_30 min

a) Eastern North America Sites

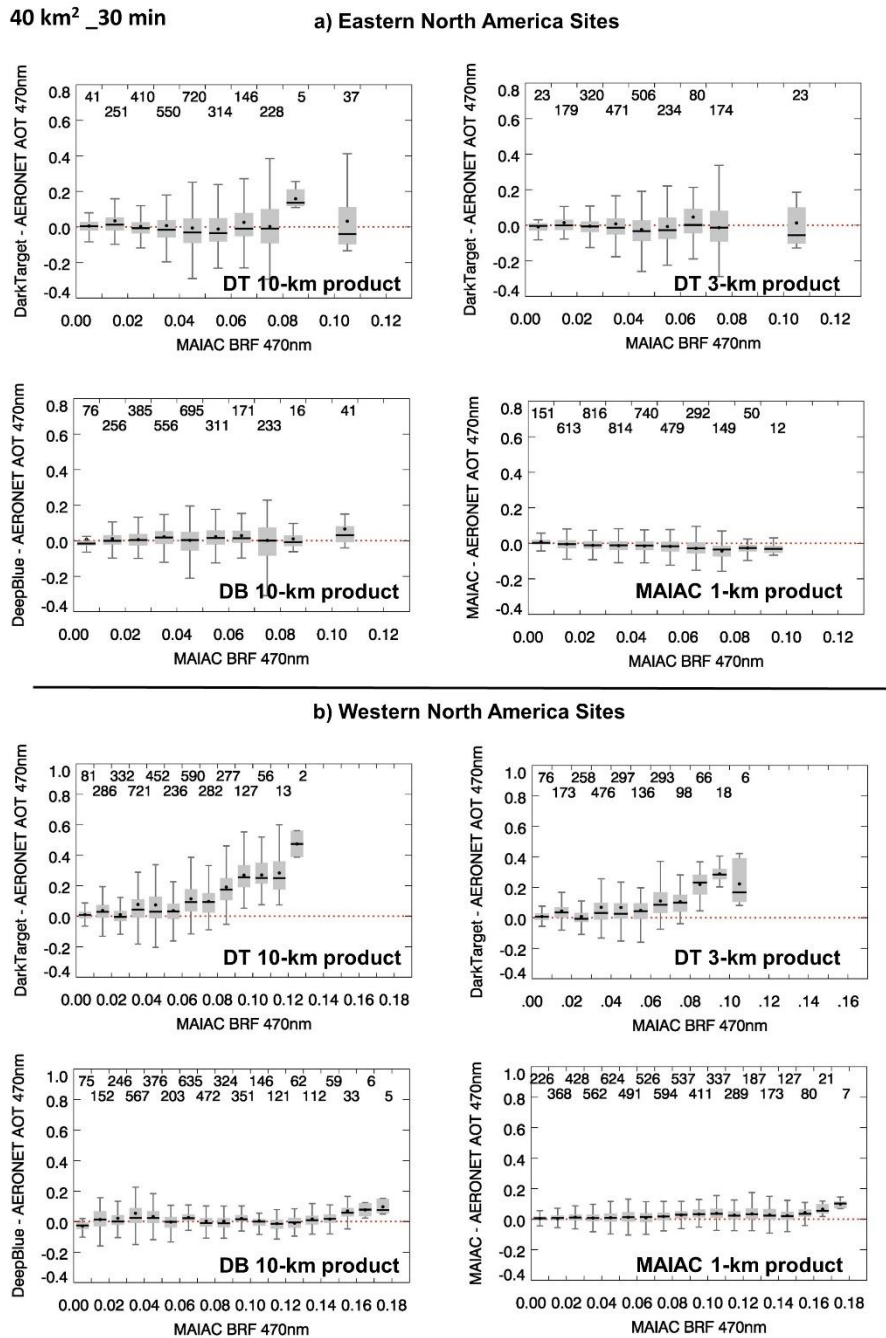


b) Western North America Sites



**Figure 6** Difference in AOT (470 nm) between MODIS and AERONET as a function of coincident bi-directional reflectance retrievals (470 nm) from MODIS-MYD09 product for eastern NA (a, top) and western NA (b, bottom). Data are represented as a box-and-whisker plot with the thick horizontal line as the median, black dot as mean, shaded boxes are covering 75 and 25 percentiles, and vertical lines as 1.5 times the interquartile range (25-75 percentile). The number of matchups for each bin is given at the top of the plot.

# Supplementary Figure



**Supplementary Figure 1** Difference in AOT (470 nm) between MODIS and AERONET as a function of coincident bi-directional reflectance retrievals (470 nm) from MODIS-MAIAC product for eastern NA (a, top) and western NA (b, bottom). Data are represented as a box-and-whisker plot with the thick horizontal line as the median, black dot as mean, shaded boxes are covering 75 and 25 percentiles, and vertical lines as 1.5 times the interquartile range (25-75 percentile). The number of matchups for each bin is given at the top of the plot.